Transformation by Rabi oscillation of the photoelectron momentum distribution produced by oppositely circularly polarized laser pulses

E. L. Fulton and J. M. Ngoko Djiokap*
Department of Physics and Astronomy, University of Nebraska, Lincoln, Nebraska 68588-0299, USA

(Received 2 July 2024; accepted 18 November 2024; published 9 December 2024)

We report on the potential of coherent Rabi-type dynamics and the formation of the Autler-Townes (AT) doublet to dramatically transform the patterns emerging in the photoelectron momentum distribution (PMD) produced in resonant two-photon ionization of the hydrogen atom by means of *ab initio* time-dependent Schrödinger equation calculations. When this nonlinear process is driven by a single circularly polarized (CP) laser pulse with a duration longer than the Rabi period, the AT doublet is shown to modulate the circular symmetric pattern in the PMD and yield two concentric bands. When a second CP laser pulse with opposite helicity acts in a synchronous way, the twofold quadrupolar pattern in the PMD sunders to yield two parts (slow and fast electrons), with each inheriting the C_2 rotational symmetry. When the two pulses are gradually separated in time, the twofold quadrupolar asunder patterns reported for zero time delay then rotate to produce parted spirals, whose direct visualization in the PMD may be impeded by the significant intensity of the AT minimum as revealed by the azimuthal angle-integrated energy distribution as well as by distortions from detuning the laser frequency. As the superposition of two quantum states is the basis of charge migration activities in matter, these spirals-asunder, persisting among a range of pulse parameters, provide an avenue for revealing charge migration in complex systems.

DOI: 10.1103/PhysRevA.110.063105

I. INTRODUCTION

The idea of optimal and coherent laser control of ionization processes is to exploit the laser radiation properties to favor a specific outcome when several output ionization channels are accessible [1]. Laser pulse properties commonly exploited include envelope shape, carrier frequency, carrier-envelope phase, chirp, duration, the number of pulses and the time delays between them, intensity, and polarization state. While optimal control relies on pulse shaping effects [2–5], coherent control is based on quantum interference effects between several quantum pathways that are used to modulate a specific channel [6]. In temporal quantum coherent control, a sequence of two (or more) pulses delayed by τ are used to create multiple quantum paths, which then interfere thanks to the τ-dependent Ramsey phase [7]. This principle was used, for instance, to efficiently guide a quantum system from its initial state into a desired final continuum state [8]. Nonresonant, perturbative excitations were carried out in alkali-metal atoms (K, Na) by weak-intensity infrared pulses, in the multiphoton and perturbative regimes [8]. The energy distribution for the photoelectron was shown to present Ramsey [7] interference fringes, thus providing a direct measure of the time delay in the form of consecutive bright or dark fringes separated by $2\pi/\tau$ in atomic units.

As it regards sensitivity to the light polarization state, the use of oppositely circularly polarized pulses is transformative to the Einstein photoelectric effect in S-state atoms. In the multiphoton and perturbative regime within which time-dependent perturbation theory (PT) analysis is applicable (assuming perturbative excitation, i.e., negligible depletion of the initial state), both PT and full-dimensional time-dependent Schrödinger equation (TDSE) calculations predicted the emergence of a novel phenomenon in the angular-resolved energy spectra. The phenomenon was originally elaborated theoretically for single-photon ionization of initially S-state helium, where the counter rotating pulse pairs produce a distinct pattern of dual spiral arms in the threshold electron momentum distribution [9]. A year later, it was reported that the spiral arms are multiplied by multiphoton transitions [10]. Experimental confirmation of these results, including beyond the assumption of perturbative excitations, with respect to which they were theoretically derived, was also successfully undertaken in 2017 [11,12]. The experiments [11,12] were for K atoms using Ti:sapphire lasers with carrier frequency $\omega = 1.55$ eV, where three photons are required to overcome the ionization potential, $E_b \approx 4.2$ eV. For perturbative excitations (minimal ground-state population depletion), spirals with six arms were observed for threshold electrons, while spirals with eight arms were seen for the first above-threshold ionization (ATI) electrons.

Since then, several theoretical and experimental works on the physics of spiral in different targets, processes, and regimes (see, e.g., Refs. [13–36]) have been reported. Most pertinently to this paper, the Wollenhaupt group [11,12] conducted a trial where they inverted the population from the ground state to an excited state using a π pulse—inducing a nonperturbative excitation equivalent to one half of a Rabi cycle—and the population inversion was markedly reflected in the number of spiral arms (changing from six arms for threshold electrons to four arms) since the second laser pulse ionizes by a two-photon transition the excited state prepared by the first π pulse. That the phenomenon persists for this

*Contact author: marcelngoko@unl.edu

nonperturbative excitation suggests that it could coexist with other strong-field effects involving population dynamics, and strong modifications of the potential-energy landscape caused by the dynamic Stark effect, discovered in 1913 by Johannes Stark.

Three studies of the optical Stark effect on the vortex-like spiral pattern in the PMD of H [27,33] and Ne [22] were conducted in the UV and XUV regime ($\omega = 4$–23 eV) from moderate to strong intensity ($I_0 = 0.35$–71 PW/cm^2). If U_p stands for the quiver energy, the calculated strong-field regime parameter $\zeta \equiv U_p/\omega$ [37] values of 0.03 [22] for Ne, 0.8 for H [33], and 1.9 for H [27] indicate that these processes span the perturbative, quasiperturbative, and nonperturbative regimes, respectively. Given that the dynamic Stark effect acts upon the eigenvalues of an atom according only to the intensity envelope of the pulse instead of the instantaneous electric field, the up-shift or down-shift of the initial-state energy level in H or Ne can be accounted for by a time-dependent down-shift or up-shift ionization potential controllable with a Stark coefficient. Varying the Stark coefficient was found to cause symmetry distortion of the PMD when the s orbital of H [33] or p orbital of Ne [22] was ionized. Spectral alterations [27] included broadening, splitting, and fusion of the PMD were reported in strong-field ionization of H at the highest pulse intensities. These studies were for nonresonant carrier frequencies and were based upon strong-field approximation (SFA) calculations. In the presence of resonances, however, the dynamic Stark effect, known [38] to be observed in the Autler-Townes (AT) splitting [39], has never been studied in temporal quantum coherent control of ionization of an atom in the scheme (synchronized pair of counter-rotating circularly polarized light) where spiral patterns are expected to manifest themselves in the PMD. That combination is the focal point of this contribution.

In this paper, we deploy the QPROP package [40] to treat H atoms resonantly driven for sufficient periods of time where Rabi oscillations begin to occur in the multiphoton-perturbative regime. We use moderate intensities in the range $1-4\times10^{14}$ W/cm^2 and carrier frequencies resonant or close to resonant with the field-free transition between the $1s$ ground state and the $2p$ excited state in H, and we study the coexistence of spiral phenomena with the strong-field effect of resonant AC Stark shifting, visualized through the AT doublet. To achieve this goal, we first apply a single circularly polarized (CP) laser pulse and find that the AT doublet splits the circular symmetric pattern in the laser polarization plane into two concentric bands. Next, for two counter-rotating circularly polarized (CRCP) pulses arriving simultaneously at the target (thus forming a single linear-polarized pulse), the expected twofold quadrupole pattern is transformed by the AT doublet into a pair of these patterns separated in energy, each preserving the C_2 rotational symmetry. Finally, when gradually moving the two pulses apart in time, we find that the spiral formed in the PMD is bifurcated (clearly forming an AT doublet after averaging or integrating over angular variations) by the dipole energy associated with the resonantly coupled states. The persistence of spirals-asunder for various pulse parameters is demonstrated. The population dynamics are shown to inform differences and similarities in the rotational symmetry of sundered spirals for slow and fast electrons, which are produced under a superposition of the ground and excited states. Since the current work can be viewed as a generalization of the experimental study [41] done for K atoms with linear pulse pairs to circular pulse pairs (for the theoretically simpler H), our prediction is likely to be measurable for other targets (alkali-metal atoms or helium [42,43]) using appropriate laser-pulse properties, as prescribed by coherent control principles.

This paper is structured as follows: Section II discusses the conditions necessary to produce both the AT splitting and spirals in the PMD. Section III is dedicated to specifying our parameters and a brief description of the QPROP package method employed here to accurately calculate the PMD. Section IV presents, discusses, and analyzes the PMD when H atoms are ionized by a single CP or LP laser pulse, and then by pairs of CRCP laser pulses progressively delayed in time. Section V provides concluding remarks. Atomic units (a.u.) are used throughout the text unless otherwise specified.

II. CONDITIONS FOR OBSERVING THE AUTLER-TOWNES DOUBLET AND SPIRALS

An example of nonlinear coherent quantum dynamics, Rabi flopping occurs when a quantum system with two bound energy states is driven resonantly, i.e., at the frequency corresponding to the energy difference between the states. An interesting example is an atom or molecule with a populated, bound electronic state driven by a laser whose photon energy matches the transition energy to another bound electronic state. When the system is coupled to a continuum state, the energy distribution of the photoelectrons is cleaved, thus forming an AT doublet, see, e.g., Fig. 1. First predicted in the microwave regime in 1955 [39], the AT splitting was first observed instead in the optical regime [41,44] and even, very recently, in the XUV regime for a helium atom using a free-electron laser [42,43]. AT splitting in the XUV regime is experimentally challenging due to the difficulty in producing intense laser pulses with such photon energies but was never by any means theoretical precluded.

The AT doublet is *centered* around the photoelectron energy

$$E_0 = 2\hbar\omega - E_b - U_p \tag{1}$$

that one would anticipate from the quanta of energy of the driving source in excess of the liberating energy of the excited bound state and ponderomotive energy U_p associated with the transition. The two spectral components of the AT doublet, sitting on each side of the center, are *separated* by the energy associated with the effective Rabi frequency.

For continuously driven Rabi oscillations in an arbitrary two-level system coupled to a continuum of states, an analytical derivation performed by Kaiser *et al.* [45] within the electric-dipole, rotating wave, and Markov approximations predicted that the population can oscillate between the bound states with a modified Rabi frequency,

$$\Omega = \sqrt{|\Omega_0|^2 - \Gamma^2}, \tag{2}$$

where $\Omega_0 \equiv \sqrt{I_0}\mu$ is the base Rabi frequency, μ is the dipole coupling matrix element between the ground state $|G\rangle$ and excited state $|X\rangle$, and the parameter $\Gamma = I_0\gamma_0/2$ (with γ_0

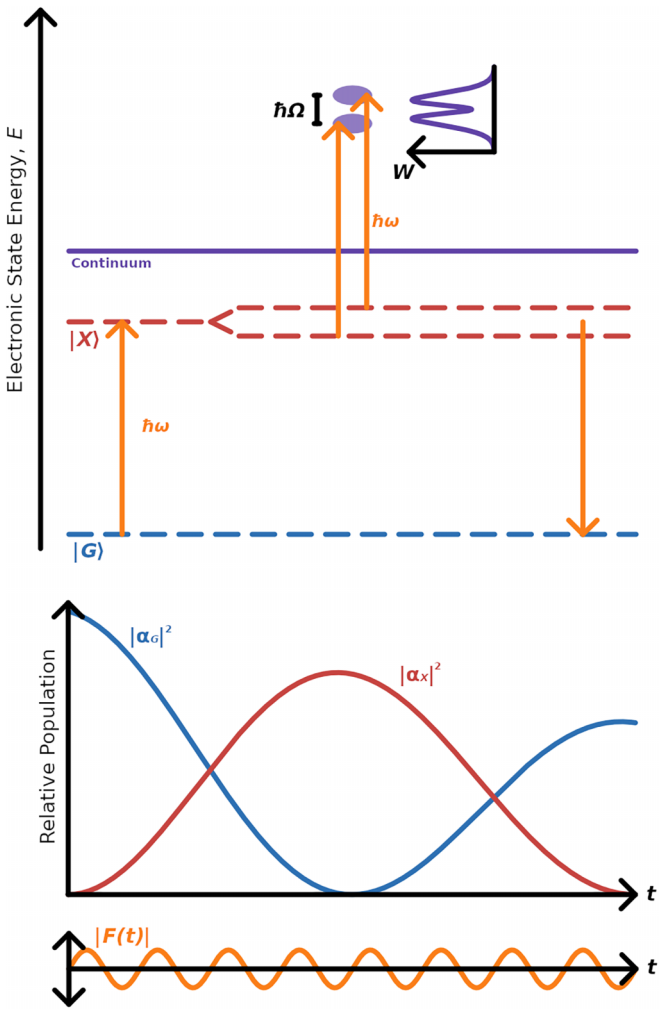

FIG. 1. Creation of Autler-Townes doublet by Rabi-type dynamics. (top) Schematic energy-band diagram for resonant two-photon ionization by a single pulse through an excited state $|X\rangle$ of an atom initially in the ground state $|G\rangle$. (middle) Rabi oscillation between ground- and excited-state populations as a function of time, shown in blue and red, respectively. Shown in the inset of the top panel is the spectroscopic splitting of the energy spectrum, known as the AT doublet, which is a direct consequence of Rabi oscillation. (bottom) Time-dependent carrier wave magnitude of the driving electric field $\mathbf{F}(t)$ (3) for a continuous wave, i.e., the envelope $f(t)$ is given by a Heaviside function.

being a constant related to the strength of interaction with the continuum) is the exponential damping coefficient on the amplitude of the oscillations due to the leaking of population to the continuum. This damping rate, which modifies the base Rabi frequency, scales linearly with the laser peak intensity I_0, while the base Rabi frequency Ω_0 scales linearly with the electric-field strength $\sqrt{I_0}$. The base Rabi frequency Ω_0 is thus the limiting case for negligible contribution from the continuum, which happens at low intensity.

In terms of the population dynamics, the Rabi period is the time required for one oscillation consisting of depletion and revival of a bound-state population. In order for the AT doublet to be formed in the energy spectra, the following three conditions must be jointly satisfied: (i) the pulse intensity I_0 must be intense enough to deplete the ground state and support Rabi oscillations through nonperturbative excitation; (ii) the total laser-pulse duration T must be long enough that the initial-state population revives, i.e., on the order of one or more effective Rabi periods, $T_R = 2\pi/\Omega$, which depends on the light polarization, envelope, etc.; and (iii) the detuning $\Delta \equiv \omega - \omega_0$ of the laser frequency ω from the field-free resonant laser frequency ω_0 must be properly chosen when intensities are strong enough to shift the atomic eigenstates. Before concluding this paragraph, it is important to highlight that if the AT doublet are formed at low intensities, then the constraint (iii) can be relaxed.

Since electron spirals are an unusual kind of Ramsey [7] interference phenomena, the energy resolution $\Delta E_{\rm res}$ of the velocity map imaging (VMI) or the cold target recoil ion momentum spectroscopy (COLTRIMS) technique for detecting the photoelectron momentum must be less than the energy gap along an azimuthal angle between successive bright or dark Ramsey interference fringes, $2\pi/\tau$. To observe spiral patterns in the PMD in the UV regime together with the AT effect requires the large bandwidth $\Delta\omega$ characteristic of ultrashort laser pulses since the bandwidth must support several Ramsey interference fringes, i.e., (iv) $\Delta E_{\rm res} < 2\pi/\tau < \Delta\omega$. This condition is effectively an upper bound on the pulse duration. One lower bound on the period is already given by condition (ii); (v) other lower bounds on the period are implicit in the need to restrict the bandwidth in order to prevent large interference between the one-photon and two-photon ionization signals, and couple effectively to a specific resonance, or at least a dominant one—though these bounds are likely less strict than what is already provided by (ii), except at extremely high intensity.

III. METHODS

We numerically investigate the confluence of the spiral-behavior of CRCP pairs of strong-field laser pulses with Rabi oscillations with respect to, for simplicity, the resonant transition from the $1s$ ground state to the $2p$ excited state in H atom. As a starting point, consider a LP pulse of moderate peak intensity 4×10^{14} W/cm^2 with a carrier frequency $\omega = 0.420$ a.u. (11.4 eV) detuned by $\Delta = 0.045$ a.u. (1.2 eV) from the field-free resonant carrier frequency $\omega_0 = 0.375$ a.u. (10.2 eV). This can naturally be constituted by two CRCP pulses each having half the field amplitude, i.e., $F_0 = 0.07549$ a.u. (note that this regards our formulation of Eq. (3) below, which incorporates the unit polarization vector; in QPROP, this is entered as $F_0 = 0.05338$ a.u., exactly half the value for LP) corresponding to a peak intensity of 10^{14} W/cm^2. We use a cosine-squared pulse envelope, i.e., $f(t) = \cos^2(\pi t/T)$, over the time range $-T/2 \leqslant t \leqslant T/2$, where T is the well-defined pulse duration. The time-dependent electric field of the first simulated laser pulse is given by

$$\mathbf{F}_1(\mathbf{e};t) = F_0 f(t) \mathrm{Re}[\mathbf{e}\, e^{-i(\omega t+\phi)}], \tag{3}$$

where ϕ is the carrier-envelope phase (CEP), $\mathbf{e}$ is the appropriate polarization vector for linear or circular light [10,14,16,37], and F_0 is the electric-field strength. Although simultaneous when constituting LP light, we later wish to separate the two CRCP pulses in time. Thus, in the later

investigations, we invoke a distinct second CP pulse given similarly to the first, except that it is delayed in time by a specified value τ and of opposite helicity, i.e., $\mathbf{F}_2 = \mathbf{F}_1(\mathbf{e}^*; t')$, where $t = t' + \tau$. The energy bandwidth associated with cosine-squared pulses can be characterized by a FWHM $\Delta\omega = 1.44\omega/N$ [10], where N is the number of laser cycles within the pulse envelope. The base Rabi frequency for this transition is, using the field-free wave functions [46],

$$\Omega_0 = F_0 \langle \Psi_{2p}|z|\Psi_{1s}\rangle = 0.745F_0. \tag{4}$$

Due, however, to the halving of intensity as averaged over the duration of the cosine-squared envelope, the pulse-lengths required are double because the population transfer is driven less strongly. Twice the ordinary Rabi period corresponding to the LP case with the intensity specified is 158 a.u., giving $N = 10.6$ laser cycles and $\Delta\omega = 1.6$ eV of pulse bandwidth at the carrier frequency $\omega = 0.420$ a.u. (11.4 eV). Because the H binding energy is $E_b = 13.6$ eV, the implication is that such a broad bandwidth pulse populates all the np excited states ($n = 2, 3, \ldots$) and even ionizes the system by one-photon transition. Nevertheless, among all these excited states, the $2p$ excited state is expected to be the main contributor, since it has the largest dipole coupling and is not in the tail of the pulse energy spectrum.

We obtain *in silico* data utilizing version 3.2 of the QPROP package [40], which is a frequently used TDSE solving package for hydrogenic atoms written in C++. Wave functions are expanded in spherical harmonics; beyond a set radius relatively far from the nucleus the Coulomb potential is approximated linearly; the photoelectron spectra can be calculated at a more distant t-SURFF boundary introduced by Tao and Scrinzi [47]. It has previously been used to investigate various PMD phenomena in H, including strong-field CRCP pulse pair-induced vortices [18] (though without simultaneous Rabi dynamics), where QPROP showed consistency with the R-matrix theory (RMT) in the range of intensities studied (up to 10^{14} W/cm^2). All photoelectron spectrum computations we performed utilize the i-SURFV method introduced for version 3 of QPROP to accelerate the PMD calculations via Green's functions. The subdirectory "vortex" in version 3 of the QPROP package is the appropriate starting point for our investigation. Computational parameters common to all results attained thereby are radial grid size: 100 a.u.; grid granularity: 0.2 a.u. (results tested for robustness at half the resolution, 0.4 a.u.); time-step size: 0.05 a.u. (results tested for robustness at half the resolution, 0.1 a.u.); potential cutoff: 25.0 a.u.; quantity of imaginary time steps: 5000; minimum t-SURFF momentum: 0.01 a.u.; momentum or energy grid scheme: equidistant in momentum; expansion scheme: 1; imaginary potential width factor: 5.0; t-SURFF boundary radius: 300.0 a.u.; imaginary potential amplitude: 100.0; number of angular momenta in expansion: 15.

IV. RESULTS

In this section, we present and discuss our numerical results on how the AT doublet produced by a single LP or CP laser pulse can affect the energy distributions (Sec. IV A) and the PMDs (Sec. IV B). Next, Sec. IV C is devoted to the case of time-delayed CRCP pulses where the observables are the PMD in both polar and rectangular representations, the energy distributions at fixed azimuthal angles, and the azimuthal angle-integrated or averaged energy distributions. Additionally, we display the time-dependent ground-state and excited-state populations to analyze the different observables.

A. Effect of Autler-Townes doublet in the photoelectron energy spectra by a single pulse

Figure 2 presents the photoelectron energy spectra (PES) of the resonant two-photon ionization of H atom driven by a single laser pulse with a carrier frequency $\omega = 11.4$ eV detuned by 1.2 eV from the field-free resonant carrier frequency $\omega_0 = 10.2$ eV, and a total duration $T = 158$ a.u. (3.8 fs) equal to twice the base Rabi period T_R. The effect of the light polarization is investigated by considering the LP case in Fig. 2(a) and the CP case in Fig. 2(b). For each case, two PES curves are shown corresponding to the strong laser intensity (nonperturbative excitation) and weak laser intensity (perturbative excitation). For better visualization, the PES at low intensities are scaled by a factor 173 for LP and 222 for CP so that they have the same height as the corresponding results for strong laser intensities. We note first that for the low intensities the quiver energy $U_p = 0.006$ eV is very small in (1) and the location of the maximum of the PES in Figs. 2(a) and 2(b) is redshifted slightly by 0.01 a.u. (0.3 eV) with respect to the expected location $E_0 = 2\omega - E_b - U_p \approx 0.25$ a.u.

Second, we would expect for perturbative excitations in the multiphoton regime that the scaling law I_0^n, where n is the number of photon absorbed, would apply. For the two-photon processes, the ionization probabilities between the weak and strong-intensity pulses would thus differ by a factor of 100^2. However, it is known and expected that the ionization probability deviates from the conventional scaling law when Rabi oscillations occur [48–51]. The significantly reduced scaling factors reported in Figs. 2(a) and 2(b) evince the nonperturbative nature of the excitation. Also, the fact that nontrivial population changes occur even for these short, moderately intense pulses, evidences that we are on or near resonance. The observed suppression of the ionization probability as laser intensity increases is attributed to Rabi oscillations [49], as can be explained by the population dynamics for the ground state and excited states.

As plotted in Fig. 3, the ground-state populations for weak laser intensity (shown as dotted curves) indicated by the curves near the top start to visually decrease from unity at around $t \approx 80$ a.u., when the amplitude of the electric field rises close to its maximum. Meanwhile, the np excited states (not shown for the weak fields) first become populated when the ground-state begins to be depleted, and then rise and fall complementary to the ground-state population. Ionization continues noticeably until around $t \approx 130$ a.u. when the laser field has been constricted by the envelope so that large population changes no longer occur. At the strong intensity, the ground-state population indicated by solid curves decreases sharply from $t = 30$ a.u. after passing through $t = 80$ a.u. and reaches a minimum (not zero because of the near-resonance nature of the process) at around $t = 90$ a.u. for the LP case. Meanwhile, the population in the np excited states, shown as red dashed line for the LP case, appears and increases in a

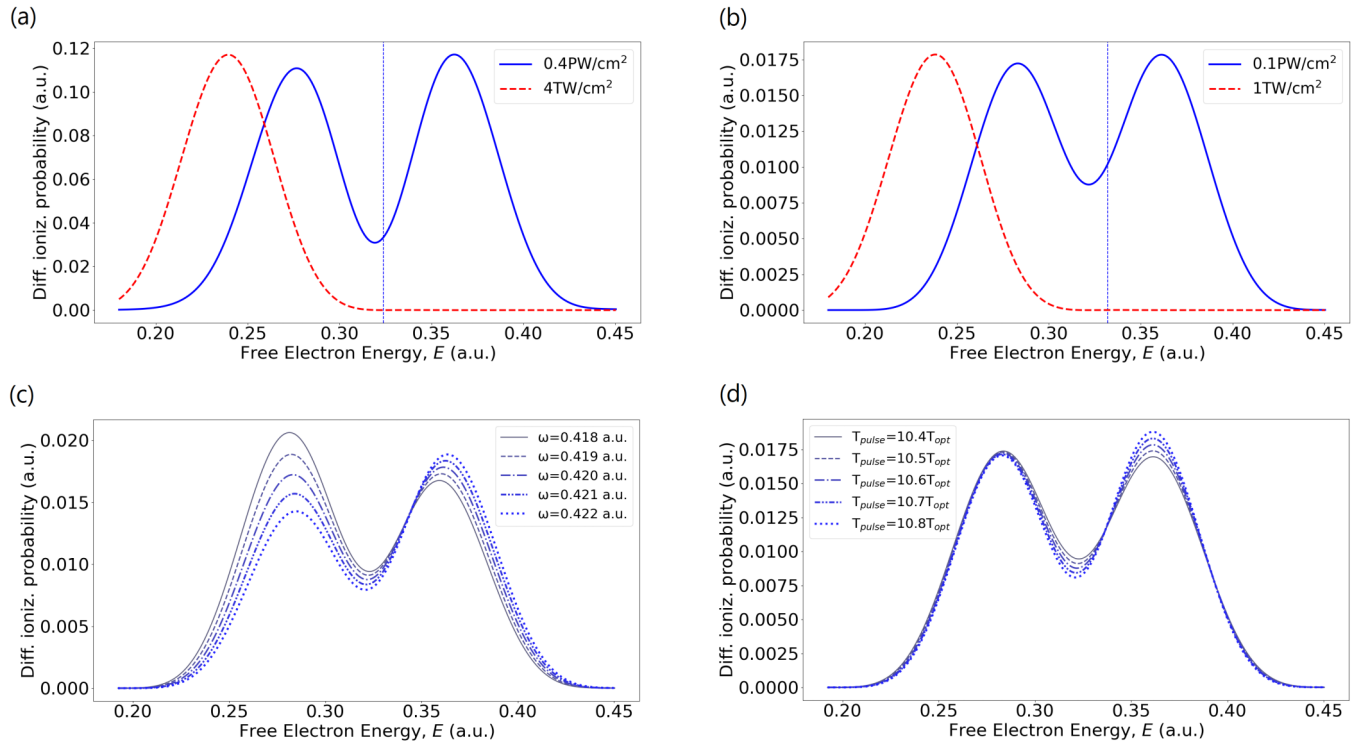

FIG. 2. Autler-Townes doublet in the photoelectron energy spectra (PES) of hydrogen atom resonantly driven by a single pulse. Shown are data obtained from simulation with the QPROP package [40] for H initially in the ground state, excited and ionized by a cosine-square enveloped pulse. (a) Linearly polarized (LP) pulse with a peak intensity of $I_0 = 4 \times 10^{14}$ W/cm^2 and (b) circularly polarized (CP) with a peak intensity four times weaker are shown in blue. Also shown in red, for comparison, are weak-field pulses without detuning (the ionization probabilities are scaled by 173 for LP and 222 for CP). Of note is that the LP light in (a) polarized along the x axis is generated by superposing two counter-rotating CP pulses of light with zero time delay at equal carrier-envelope phases (CEPs) ϕ. The pulse carrier frequency $\omega = 0.420$ a.u. (11.4 eV) is detuned from the field-free value of $\omega_0 = 0.375$ a.u. (10.2 eV) by $\Delta \equiv \omega - \omega_0 = 0.045$ a.u. (1.2 eV). As calculated for the linear case, the noninteger number of cycles of 10.6 is such that the total pulse duration of $T = 158$ a.u. (3.82 fs) is equivalent to two base Rabi periods; the Keldysh parameter is $\gamma = 3.9$ and the quiver energy for LP is $U_p = 0.44$ eV. Results shown are for the $\varphi = 0$ sliver of the light polarization plane ($\theta = \pi/2$). Note the two nearly symmetric peaks seen in panels (a) and (b) are separated by the dipole energy (2) (or approximately the base Rabi frequency Ω_0) and they do cluster around the expected kinetic energy $E_0 \approx 0.33$ a.u. given by Eq. (1) and indicated by a vertical dashed line. For the case of CP only, panels (c) and (d) show the sensitivity of the PES to the carrier frequency ω and duration T, respectively, where striking asymmetries in the size and shape of the peaks manifest.

complementary way, and becomes maximal when the ground-state population becomes minimal. From this point in time, the ground-state population starts to increase (revive) while the excited-state population decreases. These population dynamics in both the ground and excited states are a clear marker of the beginning of Rabi oscillations between the ground and several intermediate states populated by virtue of the 1.6eV pulse bandwidth (FWHM)—though the $2p$ state dominates. As in the case of the weak-field pulse, the constriction of the envelope ensures that the populations do not substantially shift beyond $t \approx 130$ a.u. Since the ionization mostly proceeds via the np excited states, the decreased probability of being in the np excited states precludes efficient ionization, which is dubbed resonance-suppressed multiphoton ionization (RSMPI). This nonperturbative behavior explains why the I_0^2 power law is no longer satisfied for our near-resonant two-photon ionization process. Of note is that if there were no ground-state population revival from its zero minimum, then the LP pulse would have been equivalent to a π pulse and the increased population in the excited state would have favored more ionization. This scheme is known as the resonance-enhanced multiphoton ionization (REMPI) [11,12]. Although precise details differ, going from the LP pulse to the CP pulse with a maximum intensity four times weaker is not transformative, as the same phenomena observed in the PES and population dynamics of the LP case occur also in the CP case.

Third, it is for only the strong laser intensities that each of the PES produced either by a LP pulse or CP pulse presents a spectroscopic splitting, with the doublet being almost symmetric in height. Scrutinizing the two local maxima of the doublet in Fig. 2(a) produced by a LP pulse along the major x axis of the polarization ellipse with electric-field strength $F_0 = 0.10676$ a.u., one sees that they are separated by 0.085 a.u., which is within 7% of the base Rabi frequency of 0.0795 a.u. obtained from Eq. (4). By contrast, the weak-field (and therefore insufficiently long) pulses show no splitting whatsoever. This structure is thus identified as the AT doublet and the agreement with theory calculated for the $2p$ state confirms its dominance among the excited states. Remarkably, for a CP pulse in the xy plane, nearly the same energy gap between the two spectral components is observed in Fig. 2(b),

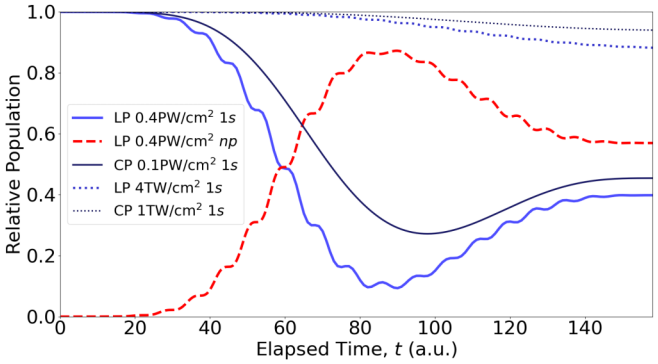

FIG. 3. Population dynamics: Time-dependent populations of the ground state $1s$ and excited states np for the pulse parameters used in Figs. 2(a) and 2(b). The different curves are described by the legend. For our cosine-squared pulse envelope and total pulse duration $T \approx 2T_R$, we note that there is near-total depletion of the ground state, followed by a substantial revival, only for the strong pulses over this time frame. The nonperturbative excitations population dynamics at $I_0 = 0.4$ PW/cm^2 for LP or $I_0 = 0.1$ PW/cm^2 for CP contrasts with the perturbative ones seen with the intensities that are two orders of magnitude smaller. For the strong-field LP case, we also show the sum of np-state populations as a dashed red line, which rise and fall complementary to the ground-state population.

reduced only down to 0.078 a.u., despite electric-field strength being $F_0 = 0.07549$ a.u. Although we would expect a larger reduction compared with the LP case, the result still agrees within a factor. Finally, the main difference between LP and CP in Figs. 2(a) and 2(b) resides in the magnitude of their AT local minima, which is higher for the CP pulse than for the LP pulse, leading to lower contrast between components.

For our near-resonant two-photon ionization process, the fact that the AT doublet observed in Figs. 2(a) and 2(b) at a detuning of $\Delta = \omega - \omega_0 \approx 0.045$ a.u. is almost symmetric for both polarizations is quite intriguing and is related to our condition (iii) discussed in the previous section. In Fig. 2(c), while keeping the other pulse parameters (duration and intensity) unchanged, we vary the carrier frequency ω of the CP pulse over a very small range from 0.418 to 0.422 a.u. as a way of examining the sensitivity of the AT doublet to the detuning. Clearly, one sees that the occurrence of the AT doublet and its local minimum location are quite robust against any small variation of ω around the central value of 0.420 a.u., where an almost symmetric doublet is seen. The local maxima are more sensitive, however, with left-right (right-left) asymmetric AT doublets emerging in the PES for ω slightly below (above) 0.420 a.u.

In Fig. 2(d), for a CP pulse of fixed carrier frequency of 0.42 a.u. and intensity of 10^{14} W/cm^2, we vary the pulse duration by slightly changing the noninteger number of laser cycles N from 10.4 to 10.8 around the reference value of $N = 10.6$ used prior, for which the total pulse duration matches twice the Rabi period. It is found that the lower spectral component of the AT doublet is very stable against such variation in N, while the higher one shows some small changes rendering the AT doublet a bit asymmetric.

B. Effect of Autler-Townes doublet in the angular-resolved energy spectra by a single pulse

Recall that the spherical angles of photoelectron momentum are the polar angle θ and azimuthal angle φ. All these PES results discussed above are for the $\varphi = 0$ sliver of the light polarization plane ($\theta = \pi/2$). As many laser cycles are required to observe the AT effect, there is no CEP effect. Next, we investigate how the AT doublet affects the azimuthal angle-resolved energy spectra and our results for the in-plane PMDs in the polar representation are shown in Fig. 4(a) for our LP pulse and in Fig. 4(b) for our CP pulse. The pulse parameters are the same as in Fig. 2. According to electric dipole selection rules, photon absorption in the $1s$ ground state causes a transition into an np excited state (with the $2p$ dominating here), which is followed by another one-photon transition into the continuum, ϵs or ϵd.

Additionally, the photon imparts magnetic angular momentum m to the electron. An LP pulse in the xy-plane drives $\Delta m = \pm 1$ transitions equally. Since we start from the $1s$ state, this means we acquire equally significant $l = 1$, $m = \pm 1$ populations. Due to the nontrivial bandwidth described by a full width at half maximum (FWHM) of $\Delta\omega = 1.6$ eV, the tail of the one-photon transition leaks a modest population of low-energy electrons into the continuum, visible in Fig. 4(a) as having a dipolar p character resulting from equal $m = \pm 1$ contributions. Meanwhile, because the electrons appearing in Fig. 4(a) at high kinetic energies can only be produced by a two-photon transition, they have a d or s character and the PMD thus exhibits a twofold quadrupole pattern, with a predominating dipole pattern along the polarization vector, which in this case is the x axis. For our near-resonant process, the two spectral components of the AT doublet simply modulate this twofold quadrupole pattern (known to occur in nonresonant two-photon ionization [10]) to yield two parts (slow and fast electrons), with each part preserving the C_2 rotational symmetry.

For a CP pulse, changes in the magnetic quantum number m are biased since m changes specifically by $+1$ (-1) when absorbing one right (left) CP photon, respectively. Therefore, while low-energy and high-energy electrons can be created by one-photon and two-photon transitions, respectively, they both appear in the PMD in the pulse polarization plane with the same shape, namely, a circularly symmetric pattern. This angular shape is explicated by the geometrical factor $e^{im\varphi}$ in the complex transition ionization amplitude acting as a global phase factor, where $m = \pm 1$ for low-energy electrons and $m = \pm 2$ for high-energy electrons. Thus, the PMD is φ-independent, explaining the circularly symmetric form. For our near-resonant process, the two spectral components of the AT doublet simply modulate this circular symmetric pattern (known to occur in nonresonant two-photon ionization [10]) to generate two concentric bands. For better visualization of the AT effect in the PMD, shown in Figs. 4(c) and 4(d) are the corresponding PMD results in Cartesian representation for high-energy (twice excited) electrons in the range 0.2 a.u. $\leqslant E \leqslant$ 0.45 a.u. We parametrized the LP pulse considered here as a superposition of two synchronous CRCP pulses, so that the patterns in Figs. 4(a) and 4(c) can serve as logical starting points for the pump-probe investigation we have conducted and

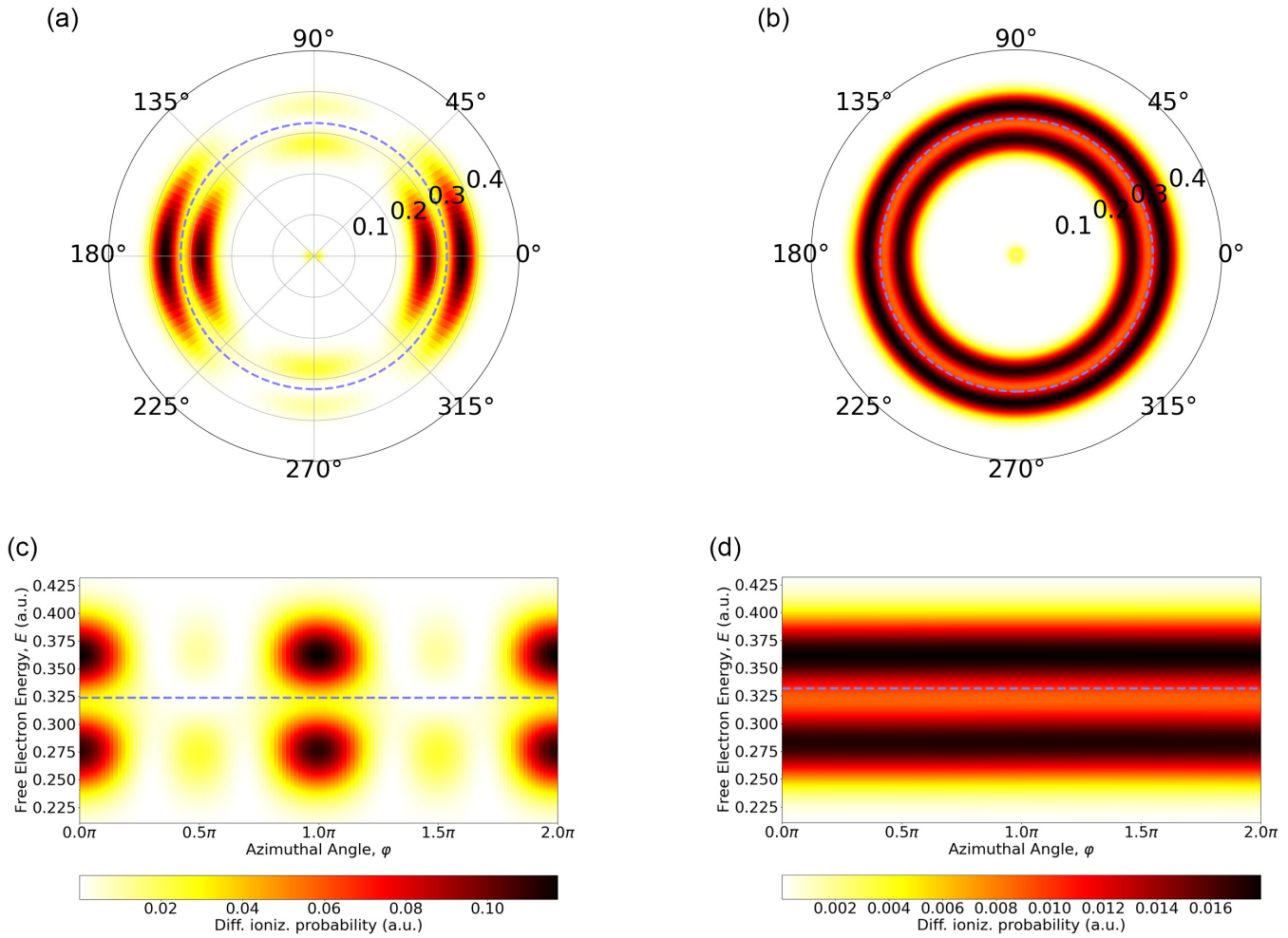

FIG. 4. Direct visualization of the Autler-Townes effect through the planar photoelectron momentum distribution (PMD) by a single pulse. (top) Polar representation for the PMDs in the polarization plane produced by a single (a) LP pulse along the x axis and (b) CP pulse with the other parameters specified in Figs. 2(a) and 2(b). An AT doublet forms near the expected central value E_0 given by Eq. (1) and indicated by a blue dashed circle. (bottom) Panels (c) and (d) are the corresponding Cartesian representation of the PMDs shown in panels (a) and (b), respectively (E_0 is now shown by a horizontal blue dashed line).

discussed below for the delayed-in-time CRCP pulse pairs.

C. Manifestation of the Autler-Townes doublet in the PMDs from time-delayed CRCP pulse pairs

The ground-state population dynamics produced by a cosine-squared CP pulse with pulse duration $T \approx 2T_R$ shown in Fig. 3 has revealed a revival phenomenon, which leads to the RSMPI process of H atoms. Let us probe such dynamics by moving our pair of CRCP pulses apart in time and taking snapshots of the produced PMD. For two CRCP overlapping laser pulses such that the ground-state depletion is negligible, there are four possible ionization paths: the two direct paths, $\Gamma_1 : 1s \to np_{+1} \to \epsilon d_{+2}$ and $\Gamma_2 : 1s \to np_{-1} \to \epsilon d_{-2}$, induced by two-photon absorption from a right-circularly polarized (RCP) and left-circularly polarized (LCP) pulse, respectively, and two pump-probe indirect paths, $\Gamma_{12} : 1s \to np_{+1} \to (\epsilon s,\ \epsilon d_0)$ and $\Gamma_{21} : 1s \to np_{-1} \to (\epsilon s,\ \epsilon d_0)$, induced by one-photon absorption from one pulse and one-photon absorption from the other pulse. The triply differential (ionization) probability (TDP) describing only the two direct paths Γ_1 and Γ_2 obtained for perturbative excitations within the PT formalism is [10]

$$\mathcal{W}(\mathbf{p}) = |\alpha(p)|^2 \sin^2(\theta) \cos^2[(\Phi + \phi_{12})/2 - 2\hat{\xi}\varphi], \quad (5)$$

which satisfy the C_4 rotational symmetry, where $\Phi = (E + E_b)\tau$ is the Ramsey interference phase accumulated between the two ionization paths, $\phi_{12} \equiv \phi_1 - \phi_2$ is the CEP difference, and $\hat{\xi} = \pm 1$ for RCP-LCP and LCP-RCP pulse pairs, respectively. When the four paths are included, the indirect paths interfere constructively (destructively) with the two direct paths to yield a pair of brighter (dimmer) spots along the major (minor) axis of the polarization ellipse for $\phi_{12} = 0$, having reduced C_2 symmetry.

Although the TDP formula (5) is derived for the case of and known to accurately describe perturbative excitation-multiphoton processes when the two CRCP laser pulses do not overlap [10], we propose here to use Eq. (5) as a way to understand the ultimate result in spite of extra dynamical effects (including massive ground-state depletion, interaction of the second pulse with a superposition of the ground state and

excited states, etc.) occurring when both optical and quantum interferences take place. The dynamical amplitude $|\alpha(p)|^2$ entering (5) is ordinarily the product of the pulse bandwidth (i.e., Fourier transform of the pulse envelope) and the radial matrix element between the ground state and the continuum but here is instead determined numerically by the energy distribution retrieved from the simulation to which we intend to compare, thereby accounting for effects of large fields and nonperturbative excitations. Using this expression (5) despite the substantial ground-state depletion, the spirals' equations in the polarization plane $\theta = \pi/2$ would be given by maxima and zeros of the kinematical factor, $\cos^2[(\Phi + \phi_{12})/2 - 2\hat{\xi}\varphi]$:

$$E^{\max,0} = \frac{4\hat{\xi}}{\tau}\varphi^{\max,0} + \frac{2k\pi}{\tau} - (E_b + \phi_{12}/\tau), \tag{6}$$

which are of Archimedean type, with k being an integer or half-integer for maxima and zeros of the TDP. Clearly, Eqs. (5) and (6) suggest that the twofold quadrupole asunder patterns (which would satisfy the C_4 rotational symmetry if the two indirect paths were to be dropped) displayed in the energy- and the azimuthal angle-resolved distribution in Fig. 4(c) may be viewed in a crude way as four-arm Archimedean spiral patterns, with slope reaching the infinite limit of $4\hat{\xi}/\tau$ as τ goes to zero.

For the same pulse parameters as in Figs. 4(a) and 4(c), we present in Fig. 5 our results for the PMDs produced by two CRCP pulses with progressively incremented time delays, namely, $\tau = T/4$ in Figs. 5(a) and 5(c), $\tau = T/2$ in Figs. 5(b) and 5(d), $\tau = 3T/4$ in Figs. 5(e) and 5(g), and $\tau = T$ in Figs. 5(f) and 5(h). For any nonzero time delays, one sees that the PMDs in the polar and Cartesian representations displayed in Fig. 5 are clearly different from the reference patterns in Figs. 4(a) and 4(c) at $\tau = 0$, i.e., produced by our LP pulse. For instance, when τ varies from zero to $T/4$ the sundered, twofold quadrupole reported for zero time delay rotates to yield two parted spirals, see Figs. 5(a) and 5(c). This rotation can be explained by the TDP (6), within which the slope $4\hat{\xi}/\tau$ of $E^{\max,0}$ varying as a function of $\varphi^{\max,0}$ is negative ($\hat{\xi} = -1$) for LRCP pulses. However, when this rotation happens, the primary and secondary dipolar patterns merge within the slow spectral component of the AT doublet, see Fig. 5(c). This behavior thus breaks down the slow-fast symmetry, leading roughly to a two-arm spiral for slow electrons, each of which branches, such that there are four arms among faster electrons, see Figs. 5(a) and 5(c). As one delays the second LCP pulse for additional increments of $T/4$ up to time delays $T/2$, as in Figs. 5(b) and 5(d), $3T/4$ as in Figs. 5(e) and 5(g), and T as in Figs. 5(f) and 5(h), not only do the bifurcated spirals continue to rotate, explainable as a weakening of the $E^{\max,0}/\varphi^{\max,0}$ slope in Figs. 5(b)–5(d), one sees that the strengths of two dipoles converge. However, there is a striking asymmetry between the four-arm spiral signal for slow and fast electrons, with the signal for slow electrons being stronger at the selected time delays for this pulse duration. Although the location of the minimum of the AT doublet is indicated in all panels in Fig. 5, the influence of Rabi dynamics in the PMD becomes increasingly difficult to parse visually. Nevertheless, the azimuthal angle-integrated energy distributions of the photoelectrons shown in Fig. 6(a) testify to the AT doublets' existence.

Analyses of Fig. 6(b) shows that the ground-state populations at zero and nonzero time delays are very different. Those differential effects are the origin of the changes in the PMDs in Figs. 4(a), 4(c), and 5 discussed above. Indeed, at $\tau = T/4$ optical interference between the two CRCP fields occurs. The resulting field is LCP from $t = 0$ to $T/4$ and RCP from $t = T$ to $t = T_f = 5T/4$, while it is a combination of LCP and RCP fields for $T/4 \leqslant t \leqslant T$, which is not linearly polarized because of the time-delay-induced phase shift inside the electric-field carrier wave and dependence of the pulse envelope. One sees that the ground-state population starts from unity and decreases sharply from $t \approx 30$ a.u., then follows the depletion path of the CP pulse reported in Fig. 3 but reaches a minimum at a time $t \approx 100$ a.u., which is about 10 a.u. later than what was reported for the LP pulse. Because the maximum of the second RCP pulse is delayed by $\tau = T/4$ with respect to the maximum of the first RCP pulse, that second pulse continues to deplete further the ground-state population (and raise the excited-state populations). These dynamical effects are followed by a quite weak revival, which indicates that ionization is more likely to be done from the excited states. As at least one-photon and two-photon absorption are required to ionize from the excited states and ground state, the symmetry breaking observed in Figs. 5(a) and 5(c) for $\tau = T/4$ suggests that the slow electrons with a two-arm spiral stem mostly from single-photon ionization of the excited state, while the fast electrons with a four-arm spiral originate mostly from two-photon ionization from the residual ground state. The situation for the slow elections is reminiscent of the π-pulse experiment carried out by the Wollenhaupt group [11,12]. Moreover, for other time delays the shapes of the ground-state population, which have stronger first revivals than the $\tau = T/4$ case [refer again to Fig. 6(b)] indicate that RSMPI by each of the sequence of two pulses occurs, meaning that ionization from the ground state becomes more favorable than ionization from the excited states. This explains why the PMDs for both slow and fast electrons in Fig. 5 for $T/2 \leqslant \tau \leqslant T$ show four distorted spiral patterns. All these results are for a pulse duration of $T =$ 158 a.u. (3.8 fs), which is twice of the base Rabi period at the LP pulse intensity, and whose population dynamics in Figs. 3 and 6 show features characteristic of a π pulse followed by a population revival. This turns out to effectively drive and support the AT doublet, which produces spirals laid asunder when two CRCP laser pulses are used. To control the AT doublet and improve its visualization in the PMD, we perform two additional pulse duration studies. In the first study shown in Fig. 7(a), T is increased by a few hundred attoseconds from 3.8 fs to find the values of $T = \tau$ that minimize the amount of right-left asymmetry reported above. We find a minimum at $T = 172$ a.u. (4.2 fs), the value to which Fig. 7(a) pertains. Comparing Fig. 7(a) and Figs. 5(f) and 5(h), for both of which $T = \tau$, one sees that the AT effect is more readily visible in the PMD for the longer nonoverlapping pulses. The right-left asymmetry reported for shorter nonoverlapping pulses disappears for the case of longer pulses, as evinced by the azimuthal angle-averaged energy distribution shown in red in Fig. 8. Also plotted in pale blue and gray in that figure are the spectra of the pattern in Fig. 7(a) along three different azimuthal rays, $\varphi = 0, 2\pi/3, 4\pi/3$ (we average over all angles in the red line, rather than integrate, so as to maintain a

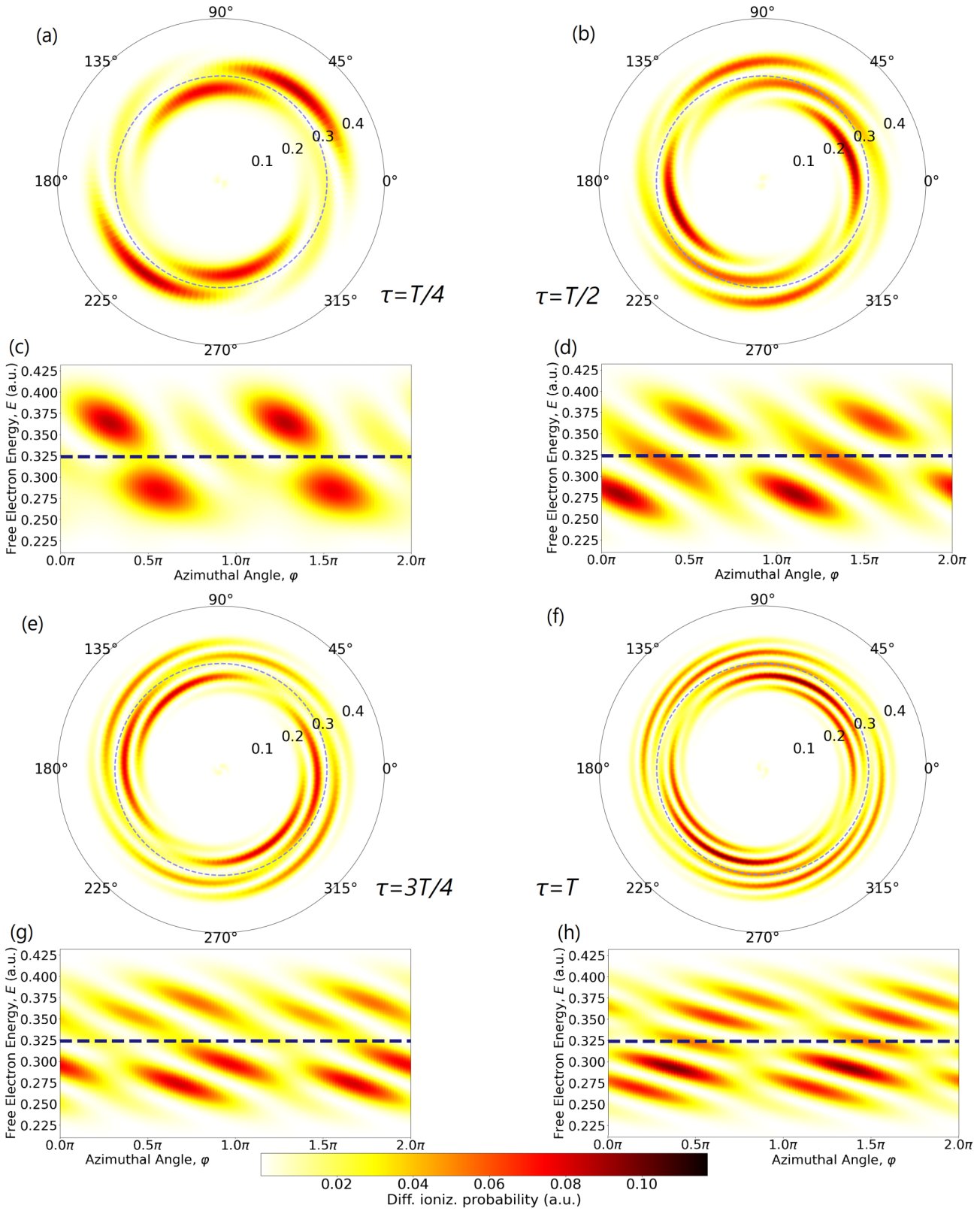

FIG. 5. Buildup and control of spirals asunder: (a), (b), (e), (f) PMDs depicted in polar representation produced by two LRCP pulses [each sharing the parameters for results shown in Fig. 2(b)] gradually separated to a time-delay of one-pulse length in four equal increments, starting at the top-left with a time delay $\tau = T/4$. Panels (c), (d) and (g), (h) are the corresponding Cartesian representation of the PMDs shown in panels (a), (b) and (e), (f), respectively, for high-energy electrons in the range 0.2 a.u. $\leqslant E \leqslant$ 0.43 a.u.

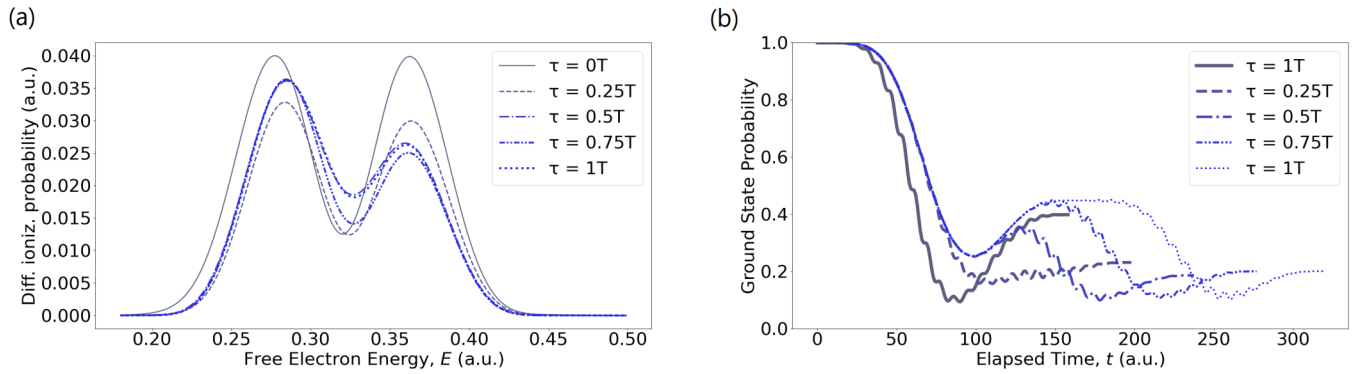

FIG. 6. Evolution of Autler-Townes doublet by Rabi dynamics across time delays: (a) Comparison of differential ionization probability in the polarization plane ($\theta = \pi/2$) integrated over φ for different time delays τ given by the legend. AT doublets are clearly visible, although of a symmetry that degrades from the initial LP case ($\tau = 0$ for our CRCP pulses). (b) Time-dependent ground-state population for the same values of τ.

consistent basis of comparison). One sees that each of these energy distributions presents some oscillatory behaviors and a bias away from the center, which we take to be a signature of the simultaneous effect of Ramsey interference and AT splitting. Because Ramsey interference is known to produce oscillatory behaviors in the energy distribution granted that τ is sufficiently long, it is only when one visualizes these photoelectron spectra in comparison with the φ-averaged (or integrated) energy distribution as a reference that the global AT effect becomes clear.

To elaborate our understanding of the spiral Ramsey interference pattern with nonperturbative excitations, we use the

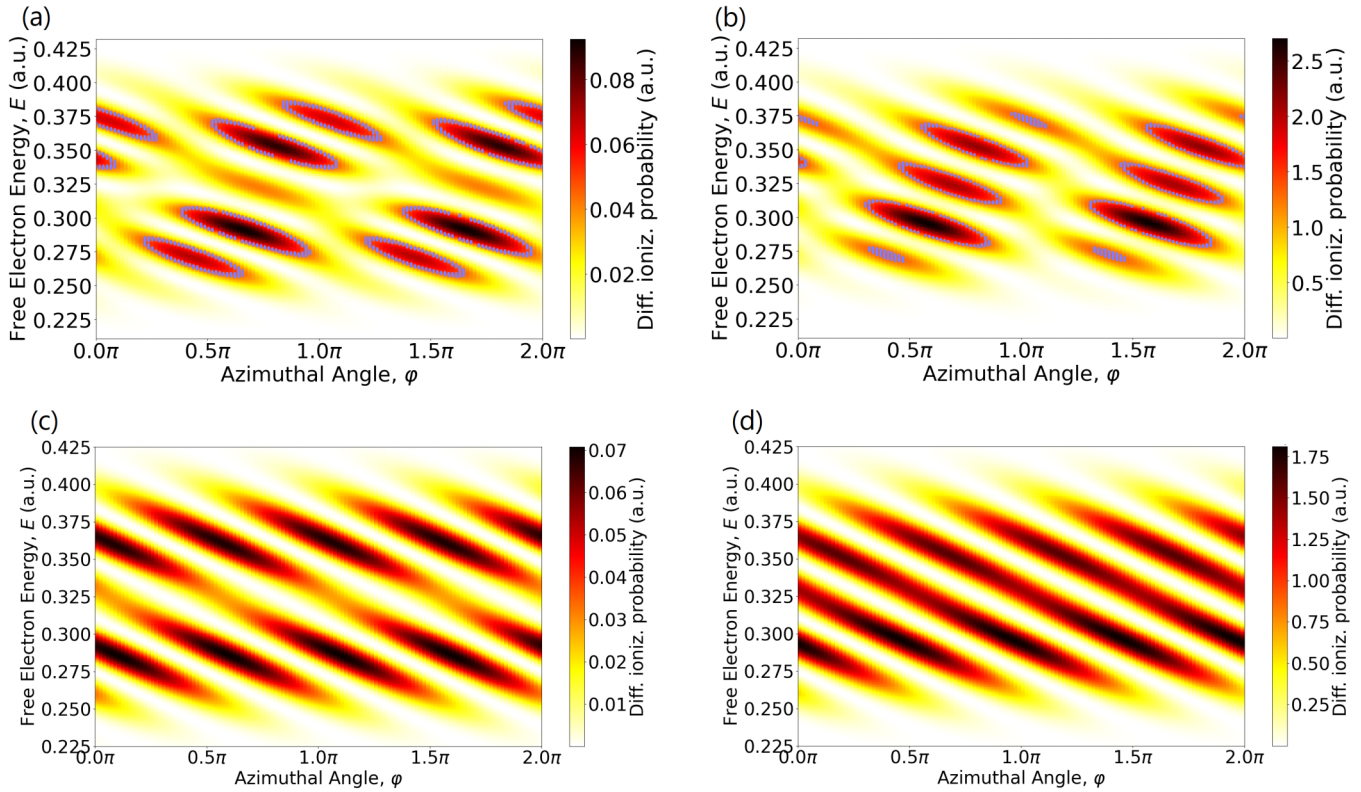

FIG. 7. Spiral pattern in confluence with Autler-Townes doublet: PMDs for pairs of nonoverlapping, CRCP pulses delayed in time by $\tau = T$, with each having a carrier frequency of $\omega = 0.420$ and a longer duration $T = 172$ a.u., corresponding to $N = 11.5$ laser cycles. (a) Simulated result for a pair of strong-field pulses with a peak intensity of $I_0 = 10^{14}$ W/cm^2 in the polarization plane ($\theta = \pi/2$). (b) PMD for two weaker pulses ($I_0 = 10^{12}$ W/cm^2) for a point of comparison. Since the Rabi period becomes much longer than the pulse duration at the weaker intensity, the Rabi dynamics do not emerge. Panels (c) and (d) are the PMDs calculated using PT formula (5) for the conjoined E, φ dependence, but with the separated function, dynamical amplitude $|\alpha(p)|^2$, given by the φ averaged energy distribution extracted from panels (a) and (b), respectively. The weak-field results in panels (b) and (d) are scaled by five orders of magnitude. To distinguish panels (a) and (b), blue contours (at 50% of the maximum TDP value for each graph) are shown, which helps to visualize the AT minimum effect in panel (a).

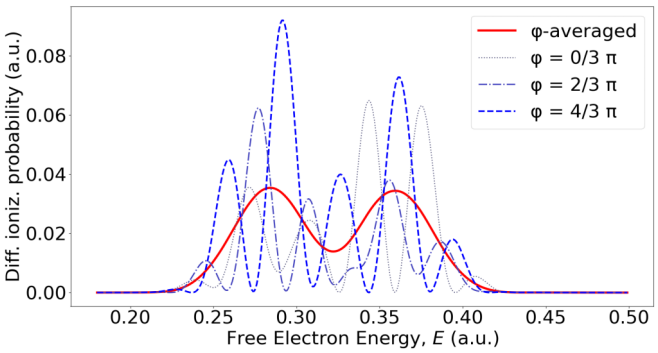

FIG. 8. AT doublet apparent in lieu of angle dependence: The azimuthal-angle φ-averaged energy spectra for the results shown in Fig. 7(a), where the AT doublet is obvious and symmetric. Also shown are the energy spectra at various specific azimuthal angle slices.

PT formula (5) to illustrate a naive theoretical PMD. Here, the dynamical parameter $|\alpha(p)|^2$ is given by the azimuthal angle-averaged energy distribution shown by the red solid curve in Fig. 8. The result of this calculation is displayed in Fig. 7(c), which is of course nonphysical because the AT effect cannot happen without the nonperturbative excitations that are beyond the scope of formula (5). However, the persistent resemblance of the basic spiral structure, contrasted with some striking differences between Figs. 7(a) and 7(c), reinforces the importance of the essential dynamics while indicating that the strong-field and or the detuning needed creates extra distortions.

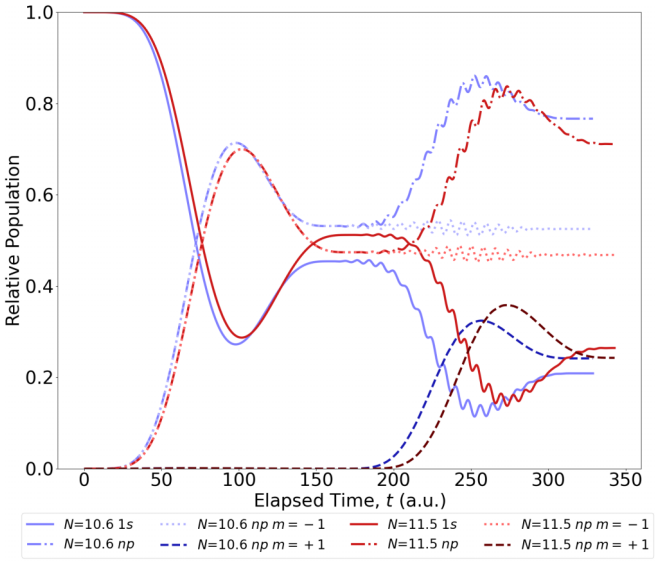

FIG. 9. Population dynamics of time-separated counter-rotating pulses. Populations for the pairs of time delayed $\tau = T$ CRCP light pulses of durations $N = 10.6, 11.5$ whose PMDs are shown in Figs. 5(f), 5(h), and 7(a), respectively. The short duration populations are shown in blue and the long in red. We distinguish between ground-state populations (solid), total np excited-state populations (dash-dot), and also the subdivisions between the $m = \pm 1$ excited states (-1 lightly dotted, $+1$ darkly dashed).

We show in Fig. 9 the ground- and excited-state populations produced by the nonoverlapping CRCP pulses of both durations discussed (10.6 and 11.5 laser pulses). The $N = 11.5$ pulses produce the more symmetric AT doublet, and we see that the balance between the ground and excited states (solid red and dash-dot red) just after the first pulse and just before the second is better than for the $N = 10.6$ pulse (blue curves) due to a deeper revival of the ground state. We additionally provide the time-series for the excited states resolved by magnetic angular momentum. We see that the $m = -1$ states are the only ones excited by the LCP pulse ($0 < t < T = 158, 172$ a.u.). The second, RCP pulse ($158, 172$ a.u. $< t < 2T$) drives population instead into the $m = +1$ state, with only minor oscillations around a constant average in the $m = -1$ state, so that at the end of the RCP pulse no more population has acquired a negative magnetic angular momentum than at the beginning of the pulse. As anticipated by the selection rules, the $m = 0$ and $l > 1$ states are irrelevant.

In the second study, whose result is shown in Fig. 7(b), we consider a weak peak intensity (10^{12} W/cm^2) to study the effect of the detuning-CRCP combination in isolation. Since the Rabi period becomes much longer than the pulse duration at this weaker intensity, the Rabi dynamics do not emerge and there is no AT effect in Fig. 7(b), as in the weak-field simulations for single pulses [refer back to Figs. 2(a), 2(b), and 3]. If this pulse intensity were low enough such that we are in the multiphoton-perturbative regime without or with negligible ground-state depletion, then only the direct ionization channels Γ_1 and Γ_2 would contribute through Ramsey interference for such nonoverlapping pulses ($T = \tau$). In such cases, a *regular* Archimedean spiral would occur in the PMD in the polarization plane and would be fully described by Eqs. (5) and (6). The irregularities observed in Fig. 7(b) demonstrate the effect of the detuning even when there is minimal ground-state depletion and the formula (5) ought to apply. We once again employ this formula to illustrate the theoretically expected PMD, where the dynamical parameter $|\alpha(p)|^2$ is given by the azimuthal angle-integrated energy distribution extracted from Fig. 7(b). The result of this calculation is shown in Fig. 7(d), which shows a regular four-arm spiral pattern without any distortion. Of note is that consecutive zeros or maxima of the energy distribution obtained from Fig. 7(d) at a fixed azimuthal angle φ are separated by $2\pi/\tau$, derivable using the valid Eq. (6). The difference between Fig. 7(b) and Fig. 7(d) highlights the compromises involved in moving towards nonperturbative excitation.

D. Robustness of the coexistence of the electron spiral and Autler-Townes doublet against changes in laser-pulse parameters

Although the conditions for observing the AT doublet and spirals are thoroughly discussed in Sec. II, here we investigate in Fig. 10 the stability of the spiral-asunder phenomena against changes to the pulse parameters, including the pulse intensity, detuning frequency, and duration. The pulses' duration in Fig. 10 is sufficiently long such that there is a mix between the dressed-states populations. The spiral phenomena always present themselves in the PMDs, where the separation

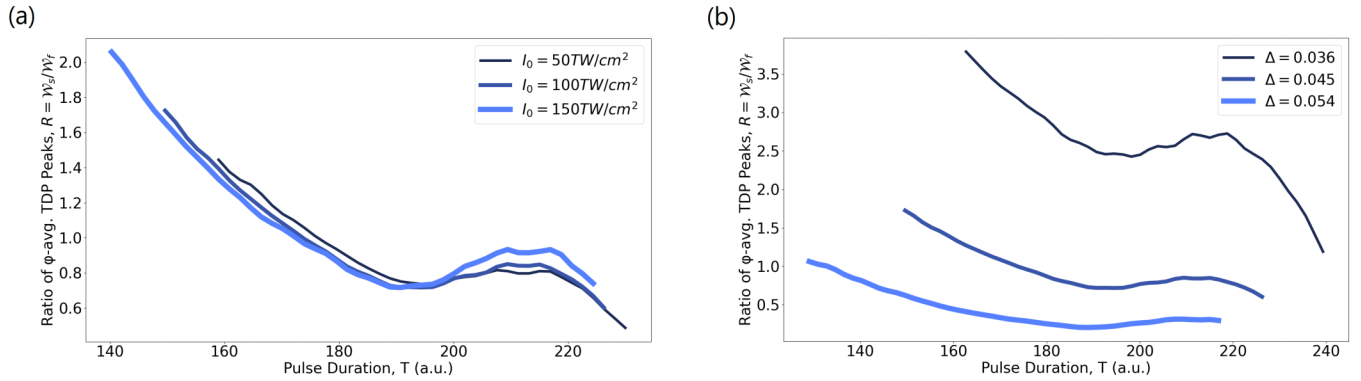

FIG. 10. Dependence of the electron spiral and the AT doublet on laser-pulse parameters. Sensitivity to the (a) pulse-pair intensity and (b) detuning of the local maxima ratio $R = \mathcal{W}_S/\mathcal{W}_F$ as a function of pulse duration. Specifically, the local maxima $\mathcal{W}_S$ and $\mathcal{W}_F$ are the azimuthal angle φ-averaged TDP peaks for the slow and fast photoelectrons in the AT doublet, respectively. The series are not plotted after reaching gaps where the peaks are no longer distinguishable. In panel (a), the carrier frequency is $\omega = 0.420$ (corresponding to a detuning of $\Delta \equiv \omega - \omega_0 = 0.045$) and three series are plotted for pulse intensities, ± 0 and $\pm 50\%$ of the intensity 100 TW/cm^2 used throughout the paper. In panel (b), the pulse intensity is held at $I_0 = 100$ TW/cm^2 and the values of the detuning, ± 0 and $\pm 20\%$ of the detuning 0.045 used throughout the paper.

between arms is well characterized by the reciprocal of the time delay (not shown). More ionization occurs for longer pulses, but to focus on the electron dynamics we introduce the dimensionless ratio, $R = \mathcal{W}_S/\mathcal{W}_F$, of the azimuthal angle φ-averaged TDP peaks for the slow and fast photoelectrons in the AT doublet. As the pulse length varies, we show below that the sensitivity to the pulse intensity or detuning frequency of this ratio R helpfully summarizes the variation of the AT splitting. In Fig. 10, we cut off each series, where the φ-averaged spectrum does not have a mathematically strict local maxima for both slow and fast photoelectrons. The AT splitting emerges once more for sufficiently long pulse durations, but we limit our scope to the range contiguous to the previously employed durations.

For a carrier frequency of $\omega = 0.420$ (corresponding to a detuning of $\Delta \equiv \omega - \omega_0 = 0.045$), Fig. 10(a) displays the variation of R as a function of the pulse duration for three values of the pulse intensity, 5×10^{13}, 10^{14}, and 1.5×10^{14} W/cm^2. Because the Rabi period is inversely proportional to the electric-field strength, the lower bound on the pulse duration that supports the sundering of the spirals is longer for the least intense pulse. Regardless of the pulse intensity, one sees that R decreases linearly with the pulse duration from a value greater than unity, demonstrating thus the left-right asymmetric AT doublet effect; it passes through unity, where the AT doublet is symmetric; next, it continues to decrease and reaches a minimum of $R \approx 0.7$ at $T \approx 195$; and then inflects to yield a concave-down parabola peaking at $T \approx 215$, although R remains below unity. $R < 1$ means that the right-left asymmetric AT doublet occurs. We conclude that the spiral asunder is quite robust against changes in the pulse intensity in the range 0.5–1.5×10^{14} W/cm^2, where both symmetric and asymmetric AT doublet effects manifest themselves for nearly the same pulse durations. This stability against the pulse intensity indicates that the shift of the atomic eigenstates is not too strong in that pulse intensity range.

Likewise, for a pulse intensity of $I_0 = 10^{14}$ W/cm^2, Fig. 10(b) shows the variation of R versus the pulse duration T for two values of the detuning frequency $\Delta \equiv \omega - \omega_0$, namely, 0.036, and 0.054. Also shown for comparison is the $\Delta = 0.045$ result, already discussed in Fig. 10(a). Clearly, one sees that the trends of variation of R with T are pretty stable and independent of the detuning frequency Δ. However, there is a strong Δ dependence for the magnitude of R. For instance, for the lowest detuning $\Delta = 0.036$, only left-right asymmetric AT doublets occur over the range of pulse intensity shown in Fig. 10(b). For the highest detuning $\Delta = 0.054$, while roughly symmetric AT doublets are formed at the lowest bound of T, there are then followed by the presence of only right-left AT doublets for longer T. The splitting of the AT doublet is not as simple as the separation of the spiral arms because it depends on both the rate of ionization of the dressed states and their populations, all of which vary on these parameters and throughout the pulse pairs.

V. SUMMARY AND CONCLUSIONS

We deployed the QPROP package [40] to study the resonant two-photon ionization of H atoms driven by laser pulses such that Rabi oscillations begin to manifest themselves in the multiphoton-perturbative regime. For three polarization schemes including a purely circularly polarized (CP) pulse and two oppositely CP pulses reaching the target simultaneously or with a time delay τ, we first found the laser properties favorable for the occurrence of the famous Autler-Townes (AT) doublet in the photoelectron energy spectra, and then showed how this can transform the photoelectron momentum distributions.

In the first two polarization cases, the apparent circularly symmetric pattern and twofold quadrupole pattern are modulated by the AT splitting to yield fast and slow copies of themselves. In the last case, where τ varies, the twofold quadrupolar asunder patterns reported for zero time delay are shown to rotate and produce parted spirals, the shape and rotational symmetry of which may differ between fast and slow spectral components. Further exploration of pulse parameters (intensity, detuning, duration) demonstrates the robustness of the coexistence of the electron spiral and AT doublet.

Population dynamics analyses have identified two ionization mechanisms, namely, the resonance-enhanced multiphoton ionization (REMPI) for π pulses and resonance-suppressed multiphoton ionization (RSMPI) for longer pulses, which provide a transparent understanding of the spirals asunder produced at different time delays.

As electron spiral phenomena were experimentally reported by the Wollenhaupt group [11,12] for nonperturbative excitations of alkali atoms by REMPI using femtosecond π pulses (i.e., half of a Rabi oscillation), our study goes beyond the half of the Rabi-type cycle dynamics. Although the experimental work [41] was based on linearly polarized IR fields exciting alkali atoms, the phenomenon we predict from simulations with CP UV fields exciting hydrogen should be measurable experimentally for alkali or other experimentally expedient atomic targets using appropriate pulse properties since the underlying dynamics studied here generalize to any resonantly coupled two-level system. In the XUV regime, two recent experiments [42,43] based on an intense free-electron laser (FEL) pulse have successfully observed the AT doublet in the He atom. What remains to be accomplished in this regime is the experimental observation of electron spirals, which have been identified as one of the scientific targets for improving the energy resolution in a novel experiment that utilizes femtosecond polarization shaping of FEL pulses [52].

ACKNOWLEDGMENTS

This work is partially supported by the U.S. Department of Energy (DOE), Office of Science, Basic Energy Sciences (BES), under Award No. DE-SC0021054 and the U.S. National Science Foundation under Grant No. PHY-2208078.

[1] V. Blanchet, C. Nicole, M.-A. Bouchene, and B. Girard, Temporal coherent control in two-photon transitions: From optical interferences to quantum interferences, Phys. Rev. Lett. **78**, 2716 (1997).

[2] B. Kohler, V. V. Yakovlev, J. Che, J. L. Krause, M. Messina, K. R. Wilson, N. Schwentner, R. M. Whitnell, and Y. J. Yan, Quantum control of wave packet evolution with tailored femtosecond pulses, Phys. Rev. Lett. **74**, 3360 (1995).

[3] A. Assion, T. Baumert, J. Helbing, V. Seyfried, and G. Gerber, Coherent control by a single phase shaped femtosecond laser pulse, Chem. Phys. Lett. **259**, 488 (1996).

[4] H. Rabitz, Strong arming molecular dynamics, Science **314**, 264 (2006).

[5] H. Rabitz, Shaped laser pulses as reagents, Science **299**, 525 (2003).

[6] M. Shapiro, J. W. Hepburn, and P. Brumer, Simplified laser control of unimolecular reactions: Simultaneous excitation, Chem. Phys. Lett. **149**, 451 (1988).

[7] N. F. Ramsey, A molecular beam resonance method with separated oscillating fields, Phys. Rev. **78**, 695 (1950).

[8] M. Wollenhaupt, A. Assion, D. Liese, Ch. Sarpe-Tudoran, T. Baumert, S. Zamith, M. A. Bouchene, B. Girard, A. Flettner, U. Weichmann *et al.*, Interferences of ultrashort free electron wave packets, Phys. Rev. Lett. **89**, 173001 (2002).

[9] J. M. Ngoko Djiokap, S. X. Hu, L. B. Madsen, N. L. Manakov, A. V. Meremianin, and A. F. Starace, Electron vortices in photoionization by circularly polarized attosecond pulses, Phys. Rev. Lett. **115**, 113004 (2015).

[10] J. M. Ngoko Djiokap, A. V. Meremianin, N. L. Manakov, S. X. Hu, L. B. Madsen, and A. F. Starace, Multistart spiral electron vortices in ionization by circularly polarized UV pulses, Phys. Rev. A **94**, 013408 (2016).

[11] D. Pengel, S Kerbstadt, D. Johannmeyer, L. Englert, T. Bayer, and M. Wollenhaupt, Electron vortices in femtosecond multiphoton ionization, Phys. Rev. Lett. **118**, 053003 (2017).

[12] D. Pengel, S. Kerbstadt, L. Englert, T. Bayer, and M. Wollenhaupt, Control of three-dimensional electron vortices from femtosecond multiphoton ionization, Phys. Rev. A **96**, 043426 (2017).

[13] K.-J. Yuan, S. Chelkowski, and A. D. Bandrauk, Photoelectron momentum distributions of molecules in bichromatic circularly polarized attosecond UV laser fields, Phys. Rev. A **93**, 053425 (2016).

[14] M. A. H. B. M. Yusoff and J. M. Ngoko Djiokap, Time delay control of reversible electron spirals using arbitrarily chirped attosecond pulses, Phys. Rev. A **109**, 023107 (2024).

[15] Z.-X. Lei1, S.-J. Yan, X.-Y. Hao, P. Ma, S.-P. Zhou, and J. Guo, The momentum distributions of triatomic molecular ion H_3^{2+} by intense laser pulses, Commun. Theor. Phys. **75**, 065501 (2023).

[16] N. J. Strandquist and J. M. Ngoko Djiokap, Reversible electron spirals by chirped attopulses at zero time delay, Phys. Rev. A **106**, 043110 (2022).

[17] L. Geng, F. Cajiao Vélez, J. Z. Kamiński, L.-Y. Peng, and K. Krajewska, Structured photoelectron distributions in photodetachment induced by trains of laser pulses: Vortices versus spirals, Phys. Rev. A **104**, 033111 (2021).

[18] A. S. Maxwell, G. S. J. Armstrong, M. F. Ciappina, E. Pisanty, Y. Kang, A. C. Brown, M. Lewenstein, and C. Figueira de Morisson Faria, Manipulating twisted electrons in strong-field ionization, Faraday Discuss. **228**, 394 (2021).

[19] J. M. Ngoko Djiokap, Atomic photoionization by multiple temporal pairs of slits, Phys. Rev. A **104**, 013115 (2021).

[20] J. M. Ngoko Djiokap, A. V. Meremianin, and N. L. Manakov, Electron interference in atomic ionization by two crossing polarized ultrashort pulses, Phys. Rev. A **103**, 023103 (2021).

[21] K. Eickhoff, L. Englert, T. Bayer, and M. Wollenhaupt, Multichromatic polarization-controlled pulse sequences for coherent control of multiphoton ionization, Front. Phys. **9**, 675258 (2021).

[22] Y. He, G. Zhang, J. Tang, X. Ding, and J. Yao, Optical-stark induced distortions in vortex momentum distributions of *p*-orbital electrons of neon atoms, IEEE Photonics J. **12**, 6101209 (2020).

[23] S. Ben, S. Chen, C.-R. Bi, J. Chen, and X.-S. Liu, Investigation of electron vortices in time-delayed circularly polarized laser pulses with a semiclassical perspective, Opt. Express **28**, 29442 (2020).

[24] Z. Chen and F. He, Interference of nuclear wave packets carrying different angular momenta in the dissociation of H_2^+

in strong circularly polarized laser pulses, Phys. Rev. A **102**, 033107 (2020).
[25] H.-F. Cui and X.-Y. Miao, Photoelectron momentum distributions of single-photon ionization under a pair of elliptically polarized attosecond laser pulses, Chin. Phys. B **29**, 074203 (2020).
[26] L. Geng, F. Cajiao Vélez, J. Z. Kamiński, L.-Y. Peng, and K. Krajewska, Vortex structures in photodetachment by few-cycle circularly polarized pulses, Phys. Rev. A **102**, 043117 (2020).
[27] M. Li, G. Zhang, X. Ding, and J. Yao, AC Stark effect on vortex spectra generated by circularly polarized pulses, IEEE Photonics J. **11**, 3300111 (2019).
[28] S. Kerbstadt, K. Eickhoff, T. Bayer, and M. Wollenhaupt, Odd electron wave packets from cycloidal ultrashort laser fields, Nat. Commun. **10**, 658 (2019).
[29] S. Kerbstadt, T. Bayer, K. Eickhoff, and M. Wollenhaupt, Control of free electron wave packets by polarization-tailored ultrashort bichromatic laser fields, Adv. Phys.: X **4**, 1672583 (2019).
[30] X.-R. Xiao, M.-X. Wang, H. Liang, Q. Gong, and L.-Y. Peng, Proposal for measuring electron displacement induced by a short laser pulse, Phys. Rev. Lett. **122**, 053201 (2019).
[31] X. Kong, G. Zhang, M. Li, T. Wang, X. Ding, and J. Yao, Odd-fold-symmetric spiral momentum distributions and their stark distortions in hydrogen, J. Opt. Soc. Am. B **35**, 2163 (2018).
[32] M. Li, G. Zhang, T. Zhao, X. Ding, and J. Yao, Electron vortices in photoionization by a pair of elliptically polarized attosecond pulses, Chin. Opt. Lett. **15**, 120202 (2017).
[33] M. Li, G. Zhang, X. Kong, T. Wang, X. Ding, and J. Yao, Dynamic Stark induced vortex momentum of hydrogen in circular fields, Opt. Express **26**, 878 (2018).
[34] Z. L. Li, Y. J. Li, and B. S. Xie, Momentum vortices on pairs production by two counter-rotating fields, Phys. Rev. D **96**, 076010 (2017).
[35] J. M. Ngoko Djiokap and A. F. Starace, Doubly-excited state effects on two-photon double ionization of helium by time-delayed, oppositely circularly-polarized attosecond pulses, J. Opt. (Bristol, UK) **19**, 124003 (2017).
[36] J. M. Ngoko Djiokap, A. V. Meremianin, N. L. Manakov, S. X. Hu, L. B. Madsen, and A. F. Starace, Kinematical vortices in double photoionization of helium by attosecond pulses, Phys. Rev. A **96**, 013405 (2017).
[37] E. A. Pronin, A. F. Starace, M. V. Frolov, and N. L. Manakov, Perturbation theory analysis of attosecond photoionization, Phys. Rev. A **80**, 063403 (2009).
[38] T. Bayer, K. Eickhoff, D. Köhnke, and M. Wollenhaupt, Phase control of the autler-townes doublet in multistate systems, Phys. Rev. A **108**, 033111 (2023).
[39] S. H. Autler and C. H. Townes, Stark effect in rapidly varying fields, Phys. Rev. **100**, 703 (1955).
[40] V. Tulsky and D. Bauer, QPROP with faster calculation of photoelectron spectra, Comput. Phys. Commun. **251**, 107098 (2020).
[41] M. Wollenhaupt, A. Assion, O. Bazhan, C. Horn, D. Liese, C. Sarpe-Tudoran, M. Winter, and T. Baumert, Control of interferences in an Autler-Townes doublet: Symmetry of control parameters, Phys. Rev. A **68**, 015401 (2003).
[42] S. Nandi, E. Olofsson, M. Bertolino, S. Carlström, F. Zapata, D. Busto, C. Callegari, M. Di Fraia, P. Eng-Johnsson, R. Feifel *et al.*, Observation of Rabi dynamics with a short-wavelength free-electron laser, Nature (London) **608**, 488 (2022).
[43] F. Richter, U. Saalmann, E. Allaria, M. Wollenhaupt, B. Ardini, A. Brynes, C. Callegari, G. Cerullo, M. Danailov, A. Demidovich *et al.*, Strong-field quantum control in the extreme ultraviolet using pulse shaping, arXiv:2403.01835.
[44] T. Hänsch, R. Keil, A. Schabert, C. Schmelzer, and P. Toschek, Interaction of laser light waves by dynamic stark splitting, Z. Phys. A: Hadrons Nucl. **226**, 293 (1969).
[45] B. Kaiser, A. Brand, M. Glässl, A. Vagov, V. M. Axt, and U. Pietsch, Photoionization of resonantly driven atomic states by an extreme ultraviolet-free-electron laser: Intensity dependence and renormalization of Rabi frequencies, New J. Phys. **15**, 093016 (2013).
[46] H. M. Tetchou Nganso, Y. V. Popov, B. Piraux, J. Madroñero, and M. G. K. Njock, Ionization of atoms by strong infrared fields: Solution of the time-dependent Schrödinger equation in momentum space for a model based on separable potentials, Phys. Rev. A **83**, 013401 (2011).
[47] L. Tao and A. Scrinzi, Photo-electron momentum spectra from minimal volumes: The time-dependent surface flux method, New J. Phys. **14**, 013021 (2012).
[48] X. Zhang, Y. Zhou, Y. Liao, Y. Chen, J. Liang, Q. Ke, M. Li, A. Csehi, and P. Lu, Effect of nonresonant states in near-resonant two-photon ionization of hydrogen, Phys. Rev. A **106**, 063114 (2022).
[49] T. Sako, J. Adachi, A. Yagishita, M. Yabashi, T. Tanaka, M. Nagasono, and T. Ishikawa, Suppression of ionization probability due to Rabi oscillations in the resonance two-photon ionization of He by EUV free-electron lasers, Phys. Rev. A **84**, 053419 (2011).
[50] T. Sato, A. Iwasaki, K. Ishibashi, T. Okino, K. Yamanouchi, J. Adachi, A. Yagishita, H. Yazawa, F. Kannari, M. Aoyma *et al.*, Determination of the absolute two-photon ionization cross section of He by an XUV free electron laser, J. Phys. B: At., Mol. Opt. Phys. **44**, 161001 (2011).
[51] N. Miyauchi, J. Adachi, A. Yagishita, T. Sako, F. Koike, T. Sato, A. Iwasaki, T. Okino, K. Yamanouchi, K. Midorikawa *et al.*, Three-photon double ionization of Ar studied by photoelectron spectroscopy using an extreme ultraviolet free-electron laser: Manifestation of resonance states of an intermediate Ar^+ ion, J. Phys. B: At. Mol. Opt. Phys. **44**, 071001 (2011).
[52] G. Perosa, J. Wätzel, D. Garzella, E. Allaria, M. Bonanomi, M. B. Danailov, A. Brynes, C. Callegari, G. De Ninno, A. Demidovich *et al.*, Femtosecond polarization shaping of free-electron laser pulses, Phys. Rev. Lett. **131**, 045001 (2023).